VIP ***The following Communications have been judged by at least two referees to be "very important papers" and will be published online at www.angewandte.org soon:***

Z.-C. Wang, N. Dietl, R. Kretschmer, T. Weiske, M. Schlangen, H. Schwarz**
Catalytic Redox Reactions in the CO/N_2O System Mediated by the Bimetallic Oxide-Cluster Couple $AlVO_3^+/AlVO_4^+$

*C. D. N. Gomes, O. Jacquet, C. Villiers, P. Thuéry, M. Ephritikhine, T. Cantat**
A Diagonal Approach to Chemical Recycling of Carbon Dioxide: New Organocatalytic Transformation for the Reductive Functionalization of CO_2

Author Profile

"I like refereeing because I learn about the latest progress in the research field much earlier than others. The greatest scientific advance in the next decade will be clothes that can perform photosynthesis …"
This and more about Zhang-Jie Shi can be found on page 11566.

Zhang-Jie Shi ____ **11566**

News

Prizes from the Real Sociedad Española de Química ____ **11567 – 11568**


M. Vallet Regí


F. Maseras


A. Llobet


H. García


M. Alcarazo


E. Hevia


D. G. Rodríguez


A. Mateo-Alonso


C. Griesinger


D. Amabilino

Books

The Group 13 Metals Aluminium, Gallium, Indium and Thallium — Simon Aldridge, Anthony J. Downs — *reviewed by G. Linti* ____ **11569**

Contents

Highlights

Fuel Cells

D. S. Su,* G. Sun* ____ 11570 – 11572

Nonprecious-Metal Catalysts for Low-Cost Fuel Cells

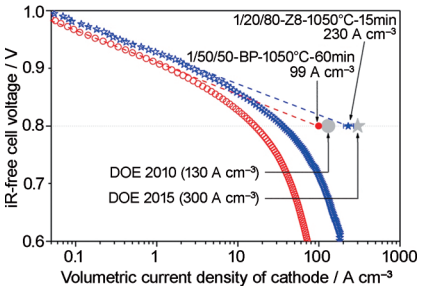

Within reach: Newly developed non-precious-metal catalysts can be used to produce inexpensive hydrogen fuel cells with performances approaching those of platinum-based systems. For example, the best non-Pt catalyst was prepared from a metal–organic framework consisting of zeolitic Zn^{II} imidazolate which served as the host for the Fe and N precursors of the catalyst. The plot shows the volumetric current densities of the best non-Pt catalysts and the target value set by the U.S. DOE at 0.8 V).

Receptor Structures

P. Kolb,* G. Klebe* ____ 11573 – 11575

The Golden Age of GPCR Structural Biology: Any Impact on Drug Design?

Keep 'em coming: Seven years after the first G-protein-coupled receptor structure was published (rhodopsin in 2000), the β_2-adrenergic receptor was the second GPCR to succumb to crystallization. Since then, a flurry of new structures, now totaling 39 structures of seven receptors, have been reported. Each structure has taught us something new about GPCR structure and activation, and it will be exciting to see what future structures will reveal.

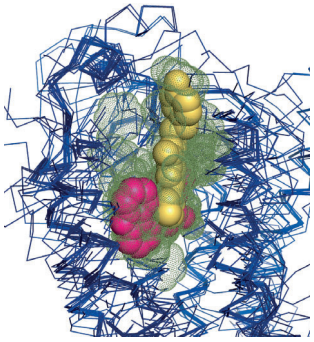

Gold Complexes

I. Krossing* ____ 11576 – 11578

Gold(I)-1,3-Diene Complexes: Connecting Structure, Bonding, and Reactivity

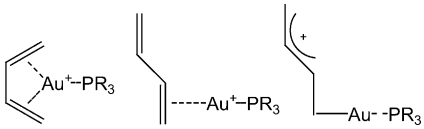

Diene to know: The gold(I)-catalyzed hydroamination reaction of dienes is influenced by the interaction mode of the $\{R_3PAu\}^+$ moiety with the diene (see picture). The recent findings of Russell, McGrady, and co-workers are put into a wider perspective, including, which coordination mode is preferred and why, how substituents influence the structure, and what the consequences for catalysis are.

For the USA and Canada:
ANGEWANDTE CHEMIE International Edition (ISSN 1433-7851) is published weekly by Wiley-VCH, PO Box 191161, 69451 Weinheim, Germany. Air freight and mailing in the USA by Publications Expediting Inc., 200 Meacham Ave., Elmont, NY 11003. Periodicals postage paid at Jamaica, NY 11431. US POSTMASTER: send address changes to *Angewandte Chemie*, Journal Customer Services, John Wiley & Sons Inc., 350 Main St., Malden, MA 02148-5020. Annual subscription price for institutions: US$ 11.738/10.206 (valid for print and electronic / print or electronic delivery); for individuals who are personal members of a national chemical society prices are available on request. Postage and handling charges included. All prices are subject to local VAT/sales tax.

Essays

The enigma of "activated acetic acid", the acetylated form of coenzyme A that participates in key metabolic processes, was solved by Feodor Lynen in 1950. The worldwide interest in this discovery led Lynen and biochemistry in Germany back into the world of international science. Lynen received the Nobel Prize in Physiology or Medicine in 1964 for his basic "discoveries concerning the mechanism and regulation of the cholesterol and fatty acid metabolism".

History of Science

H. Will,* B. Hamprecht — **11580 – 11584**

"Everything Now Seemed So Simple to Me ...": Feodor Lynen (1911–1979), a Hero of Biochemistry

Minireviews

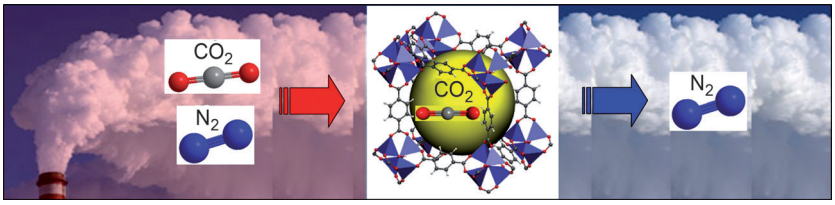

Looking for holes: How can new microporous materials, such as metal–organic frameworks (MOFs, see picture), be quickly evaluated for their practical application in CO_2 separation processes? Five adsorbent evaluation criteria are used to assess over 40 MOFs for their potential in natural gas purification, landfill gas separation, and capture of CO_2 from power-plant flue gas. Comparisons with other materials such as zeolites are made.

Carbon Dioxide Capture

Y.-S. Bae, R. Q. Snurr* — **11586 – 11596**

Development and Evaluation of Porous Materials for Carbon Dioxide Separation and Capture

Reviews

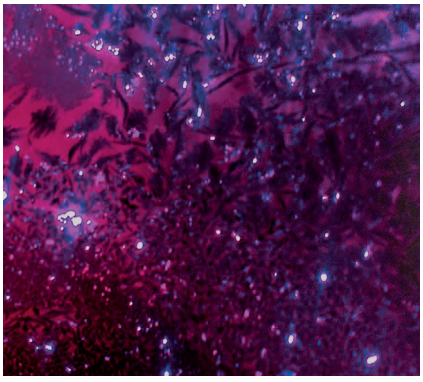

At the beginning of the 19th Century iodine (Greek ἰώδης, violet) was first obtained from brown algae by using sulfuric acid. For 200 years, iodine has played an important role in chemical research, and its significance for the environment and human health should not be underestimated. Iodine shows a versatile chemistry, is often used in organic syntheses, and has a broad spectrum of industrial applications, such as in solar cells.

History of Iodine Chemistry

F. C. Küpper,* M. C. Feiters, B. Olofsson, T. Kaiho, S. Yanagida, M. B. Zimmermann, L. J. Carpenter, G. W. Luther, III, Z. Lu, M. Jonsson, L. Kloo* — **11598 – 11620**

Commemorating Two Centuries of Iodine Research: An Interdisciplinary Overview of Current Research

Contents

Communications

Photochemistry

X. Liang, X. Li, X. Yue, Z. Dai* _____ **11622 – 11627**

Conjugation of Porphyrin to Nanohybrid Cerasomes for Photodynamic Diagnosis and Therapy of Cancer

Shining light on cancer cells: A cerasomal photosensitizer of high stability and loading efficiency was developed by conjugation of a porphyrin molecule to an organoalkoxysilylated lipid followed by sol–gel and self-assembly processes (see picture). This nanoformulation showed intrinsic fluorescence and significant damage to tumor cells under photoirradiation.

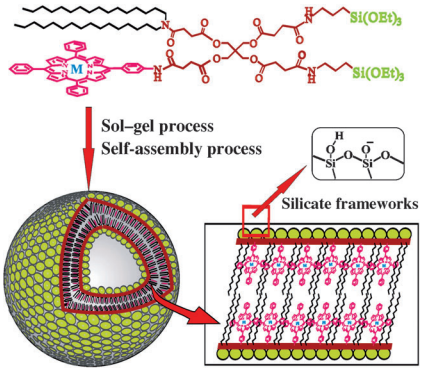

Supramolecular Photovoltaics

H. Bürckstümmer, E. V. Tulyakova, M. Deppisch, M. R. Lenze, N. M. Kronenberg, M. Gsänger, M. Stolte, K. Meerholz,* F. Würthner* _____ **11628 – 11632**

Efficient Solution-Processed Bulk Heterojunction Solar Cells by Antiparallel Supramolecular Arrangement of Dipolar Donor–Acceptor Dyes

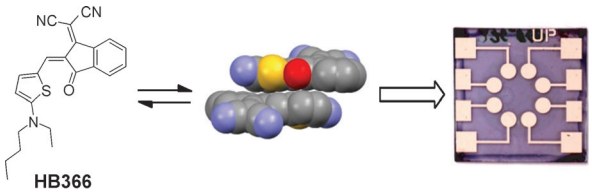

Donor–acceptor dyes with an aminothiophene donor show ideal absorption, redox, and packing features in organic photovoltaics (see picture). With blends of **HB366**:$PC_{71}BM$, highly efficient solar cells were achieved with a V_{OC} of 1.0 V, a J_{SC} of 10.2 mA cm^{-2}, and a power conversion efficiency of 4.5 %.

Drug Design

M. Reutlinger, W. Guba, R. E. Martin, A. I. Alanine, T. Hoffmann, A. Klenner, J. A. Hiss, P. Schneider, G. Schneider* _____ **11633 – 11636**

Neighborhood-Preserving Visualization of Adaptive Structure–Activity Landscapes: Application to Drug Discovery

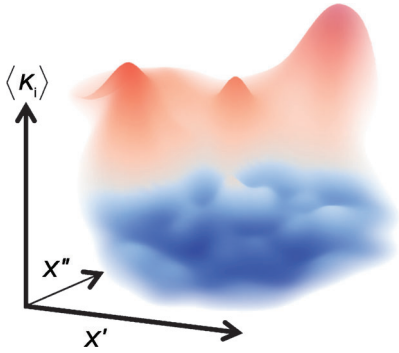

Staying fit: A computational approach that generates an intuitive visual fitness landscape (see picture; blue: possible hits, red: nonproductive hits) of chemical space that serves as a roadmap for chemical optimization of drug candidates is presented. Potential compound liabilities can be avoided, multiple properties can be considered at a time, and the information contained in both active and inactive compounds is optimally exploited.

Conformation Analysis

P. Ochsenbein, M. Bonin, K. Schenk-Joß, M. El-Hajji* _____ **11637 – 11639**

The ^2S_O Skew-Boat Conformation in L-Iduronic Acid

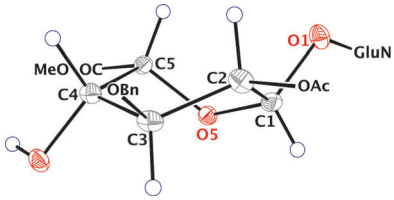

Crystal clear: After two decades of controversy the elusive skew-boat conformation of L-iduronic acid (see picture) was finally ascertained at atomic resolution in a synthetic, substituted disaccharide. This highly flexible compound crystallizes in two dimorphs. This rare case of dimorphism in oligosaccharides is all the more remarkable in that the ^2S_O conformation crystallizes in both forms.

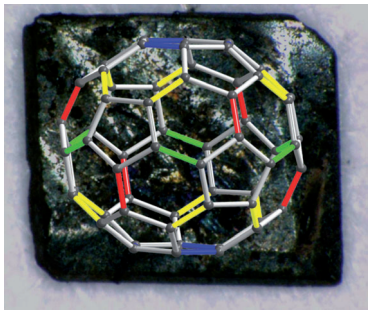

Distorted order: The synthesis and X-ray crystallographic analysis of single crystals of $[Cs(THF)_4]C_{60}$ are reported. The data obtained provide structural information sufficient to prove a Jahn–Teller distortion in the C_{60} anion radical. For the first time the transition from static to dynamic Jahn–Teller effects in fullerides has been observed directly by X-ray analysis and corroborated by magnetic measurements and EPR experiments.

Fullerides

K. Y. Amsharov, Y. Krämer, M. Jansen* ——— 11640 – 11643

Direct Observation of the Transition from Static to Dynamic Jahn–Teller Effects in the $[Cs(THF)_4]C_{60}$ Fulleride

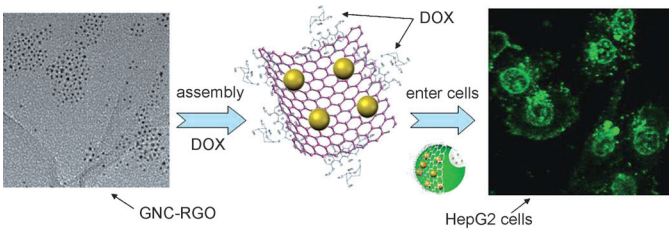

Gold and carbon make it together: Gold nanoclusters (GNCs) impregnated onto reduced graphene oxide (RGO) nanosheets cross swiftly across HepG2 hepatocarcinoma cell membranes to alter proteins and DNA and transport anticancer molecular drugs, such as doxorubicin (DOX).

Cellular Interactions

C. Wang, J. Li, C. Amatore, Y. Chen, H. Jiang, X.-M. Wang* ——— 11644 – 11648

Gold Nanoclusters and Graphene Nanocomposites for Drug Delivery and Imaging of Cancer Cells

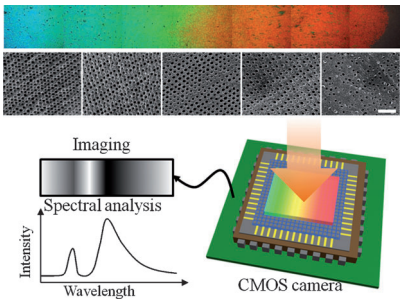

An on-chip spectrometer: Chirped 3D photonic crystals have been created using colloidal particle diffusion in a photocurable medium. The variations in the lattice constant created a color gradient that spanned the entire visible range. By combining the functionality of chirped photonic crystals with a complementary metal-oxide-semiconductor sensor array, a miniaturized spectrometer system is developed (see picture).

Photonic Crystals

S.-H. Kim,* W. C. Jeong, H. Hwang, S.-M. Yang* ——— 11649 – 11653

Robust Chirped Photonic Crystals Created by Controlled Colloidal Diffusion

A colorful bunch: Dyes based on 2,2′-biindenyl fluorophores exhibit tunable solid-state emission colors that cover the whole visible region from blue to red. The nonplanar conformation of the dyes in crystals result in bright deep-blue emission for **1**–**3**, and green emission for **4**. Furthermore, the two crystalline forms of BDY-IN (BDY-O and BDY-R) exhibit different optical properties.

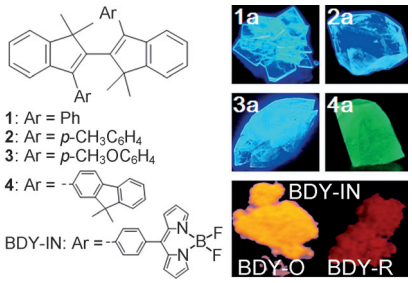

Fluorescent Dyes

Z. Zhang, B. Xu, J. Su, L. Shen, Y. Xie, H. Tian* ——— 11654 – 11657

Color-Tunable Solid-State Emission of 2,2′-Biindenyl-Based Fluorophores

Contents

Nanoparticles

J.-s. Lu, H. Fu, Y. Zhang, Z. J. Jakubek, Y. Tao, S. Wang* _____ **11658 – 11662**

A Dual Emissive BODIPY Dye and Its Use in Functionalizing Highly Monodispersed PbS Nanoparticles

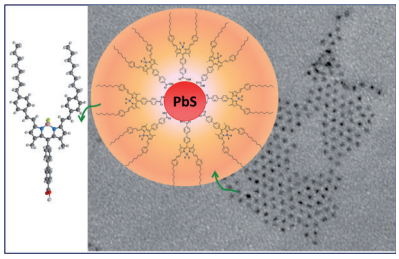

Shiny particles: A newly synthesized BODIPY dye displays unusual dual emission and can be used to functionalize highly monodisperse PbS nanoparticles (see picture; B pink, F green, O red, C gray, H white). Electronic communication between the BODIPY dye and the PbS NPs can be exploited in a photovoltaic cell.

Protein Engineering

Y. Tokita,* S. Yamada, W. Luo, Y. Goto, N. Bouley-Ford, H. Nakajima, Y. Watanabe* _____ **11663 – 11666**

Protein Photoconductors and Photodiodes

Photo finish: Zinc-substituted cytochrome b_{562} (Zn-cyt b_{562}) immobilized on a gold electrode is an n-type photodiode, whereas zinc-cytochrome c (Zn-cyt *c*) is a p-type photoconductor (see picture). DFT calculations indicate that the cytochrome band gaps are much lower than those estimated for smaller polypeptides. The semiconductor properties of these proteins depend on the charge distribution on their molecular surfaces.

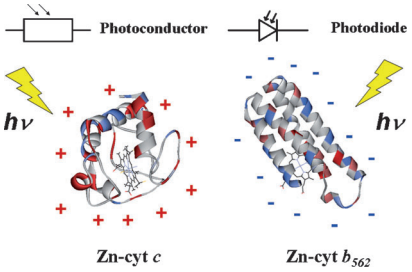

Organosilica Derivatives

M. Waki, N. Mizoshita, T. Tani, S. Inagaki* _____ **11667 – 11671**

Periodic Mesoporous Organosilica Derivatives Bearing a High Density of Metal Complexes on Pore Surfaces

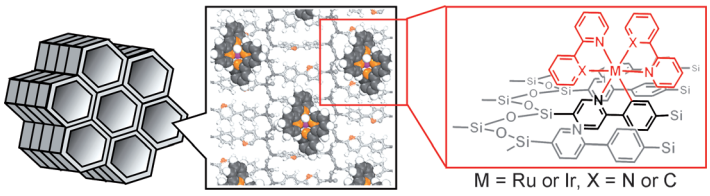

Periodic mesoporous organosilica derivatives (PMOs) that bear a high density of Ru and Ir complexes on pore walls were synthesized using a unique two-step approach: 1) synthesis of PMO containing phenylpyridine bridging groups in the pore walls, and 2) post-synthetic formation of metal complexes using the phenylpyridine groups as chelating ligands (see picture).

Isotopic Labeling

A. Gallinger, T. Biet, L. Pellerin, T. Peters* _____ **11672 – 11674**

Insights into Neuronal Cell Metabolism Using NMR Spectroscopy: Uridyl Diphosphate *N*-Acetyl-Glucosamine as a Unique Metabolic Marker

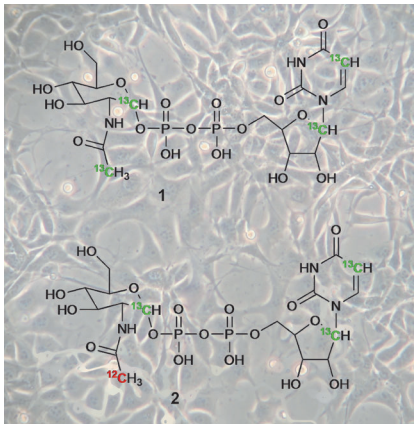

Making the switch: Compounds **1** and **2** are used as metabolic markers for NMR detection. When neuronal cells switch to a glycolytic state, an uneven distribution of ^{13}C in the N-acetyl group results, thus giving a mixture of the metabolites **1** and **2**. It is therefore possible to monitor flux through different metabolic pathways, such as glycolysis, the tricarboxylic acid cycle, and the hexosamine biosynthetic pathway, using a single molecule.

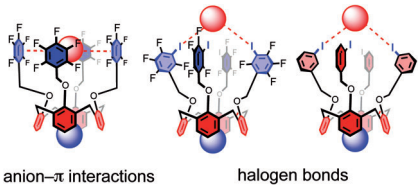

Single-atom exchange series are introduced to extract the individual contributions of halogen bonds and anion–π interactions to the transport of anions across lipid bilayer membranes (see picture). Known cation binding sites are used for counterion activation of the neutral calix[4]arene transporters. The experimental evidence for anion transport with halogen bonds is unprecedented.

Halogen Bonds

A. Vargas Jentzsch, D. Emery, J. Mareda, P. Metrangolo, G. Resnati, S. Matile* _____ **11675 – 11678**

Ditopic Ion Transport Systems: Anion–π Interactions and Halogen Bonds at Work

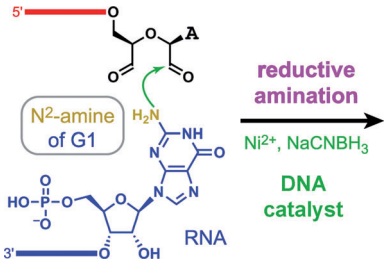

A new reaction for DNA: DNA is shown to catalyze Ni^{2+}-dependent reductive amination involving the N^2-amine of a guanosine nucleobase (see picture). This finding expands the repertoire of nucleic acid catalysis to include reductive amination, an important natural biosynthetic reaction that has practical synthetic utility.

Catalytic DNA

O. Y. Wong, A. E. Mulcrone, S. K. Silverman* _____ **11679 – 11684**

DNA-Catalyzed Reductive Amination

Good things come to those who wait: More than 160 years after their discovery, we have determined the solid-state structures of the classic organometallic compounds dimethylzinc and diethylzinc by using X-ray crystallography and density functional theory. The study shows that the linear molecules form weak intermolecular interactions with small covalent contributions. Me_2Zn undergoes a solid–solid phase transition at 180 K (see picture).

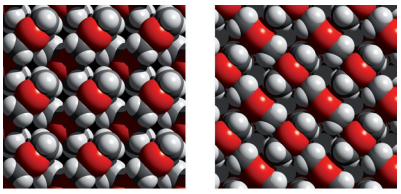

Structure Elucidation

J. Bacsa, F. Hanke, S. Hindley, R. Odedra, G. R. Darling, A. C. Jones, A. Steiner* _____ **11685 – 11687**

The Solid-State Structures of Dimethylzinc and Diethylzinc

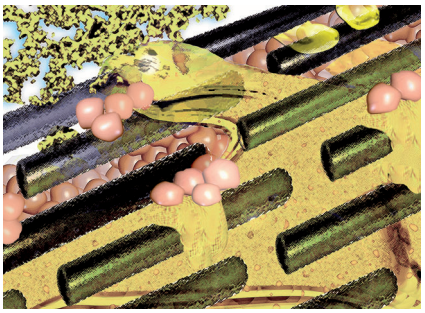

A biosilicification approach based on infiltration of fluidic choline-stabilized silicic acid precursors into polyallylamine-enriched collagen fibrils is presented. The latter serve as template and catalyst for intrafibrillar polymerization of the silica precursors to reproduce the cross-banding and microfibrillar architecture of collagen fibrils.

Intrafibrillar Silicification

L.-n. Niu, K. Jiao, Y.-p. Qi, C. K. Y. Yiu, H. Ryou, D. D. Arola, J.-h. Chen,* L. Breschi, D. H. Pashley, F. R. Tay* _____ **11688 – 11691**

Infiltration of Silica Inside Fibrillar Collagen

Contents

Helical Structures

F. Freire, J. M. Seco,* E. Quiñoá, R. Riguera* ——— **11692 – 11696**

Chiral Amplification and Helical-Sense Tuning by Mono- and Divalent Metals on Dynamic Helical Polymers

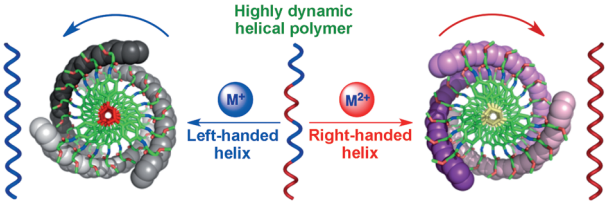

Ion sensor: A highly dynamic poly(phenylacetylene) bearing α-methoxyphenylacetic acid (MPA) as chiral pendant exhibits selective helix induction and chiral amplification, and gives a material that acts as a sensor for the valence of metal cations. Selective coordination of the pendants with mono- or divalent metal cations determines the right- or left-handed helical sense of the polymer (see picture) and its chiroptical response.

Protein ^{1}H NMR Spectroscopy

M. J. Knight, A. L. Webber, A. J. Pell, P. Guerry, E. Barbet-Massin, I. Bertini, I. C. Felli, L. Gonnelli, R. Pierattelli, L. Emsley, A. Lesage, T. Herrmann, G. Pintacuda* ——— **11697 – 11701**

Fast Resonance Assignment and Fold Determination of Human Superoxide Dismutase by High-Resolution Proton-Detected Solid-State MAS NMR Spectroscopy

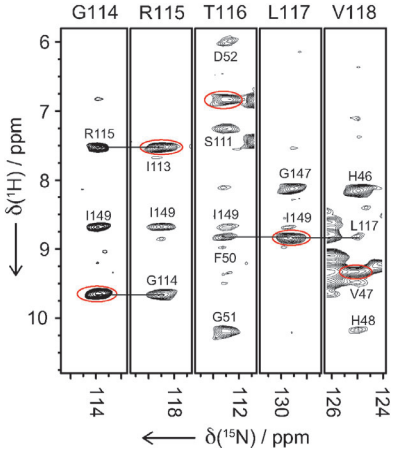

Re-protonation is key: A combination of a high magnetic field (1 GHz) and ultra-fast magic-angle spinning (60 kHz) allows easy detection of NMR spectra revealing details of secondary and tertiary structures of medium-sized proteins. The technique was applied to the 153-residue microcrystalline Zn^{II}-loaded superoxide dismutase (Zn^{II}-SOD) fully [^{2}H,^{13}C,^{15}N]-labeled and 100% re-protonated at the exchangeable sites.

Hydrogenation

E. Balaraman, Y. Ben-David, D. Milstein* ——— **11702 – 11705**

Unprecedented Catalytic Hydrogenation of Urea Derivatives to Amines and Methanol

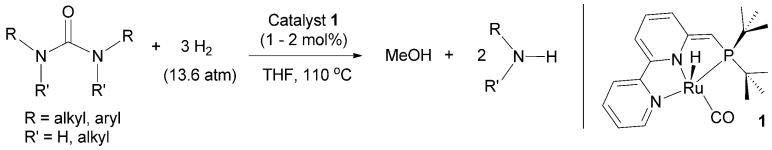

Indirect CO_2 hydrogenation: Hydrogenation of urea derivatives to the corresponding amines and methanol is reported (see picture). The reaction is catalyzed by a bipyridine-based tridentate PNN Ru(II) pincer complex and proceeds under mild, neutral conditions using 13.6 atm of H_2. A mild approach is offered for the indirect hydrogenation of CO_2 to methanol as urea derivatives are available from CO_2.

Proton Transport

D. Umeyama, S. Horike, M. Inukai, Y. Hijikata, S. Kitagawa* ——— **11706 – 11709**

Confinement of Mobile Histamine in Coordination Nanochannels for Fast Proton Transfer

Along narrow channels: Mutual integration of a microporous coordination polymer and histamine provides a proton conductivity above 10^{-3} S cm^{-1} under anhydrous conditions. Anisotropic alignment of histamine molecules in straight 1D channels creates a specific conduction pathway (see picture).

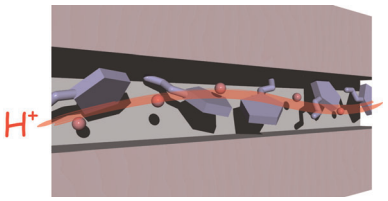

Enzyme impressionist: A DNAzyme consisting of hemin combined with a G-quadruplex was shown to mimic the activity of NADH oxidase under aerobic conditions and of NADH peroxidase under anaerobic conditions. Along with these new biocatalytic activities, the hemin/G-quadruplex complex is also capable of regenerating the biologically important NAD^+ cofactor in both cycles (see picture).

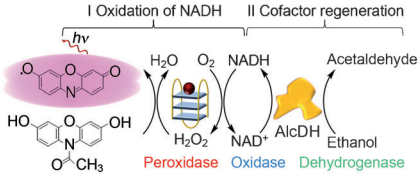

DNAzymes

E. Golub, R. Freeman, I. Willner* ——— 11710 – 11714

A Hemin/G-Quadruplex Acts as an NADH Oxidase and NADH Peroxidase Mimicking DNAzyme

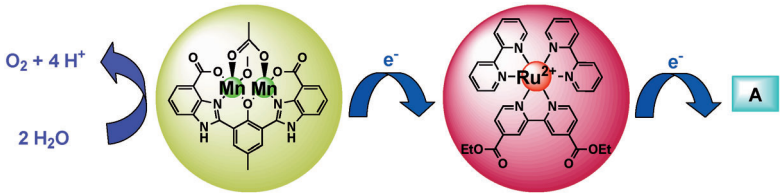

Manganificent potential: A dinuclear manganese catalyst contains metal centers that are coordinated by a central phenolate, with adjoining imidazole and carboxylate groups, which are all important functionalities in the natural oxygen-evolving center. The complex catalyzes the conversion of water to oxygen in the presence of a single-electron oxidant $[Ru(bpy)_3]^{3+}$ (see picture, bpy = 2,2′-bipyridine, A = acceptor).

Photocatalysis

E. A. Karlsson, B.-L. Lee, T. Åkermark, E. V. Johnston, M. D. Kärkäs, J. Sun, Ö. Hansson, J.-E. Bäckvall, B. Åkermark* ——— 11715 – 11718

Photosensitized Water Oxidation by Use of a Bioinspired Manganese Catalyst

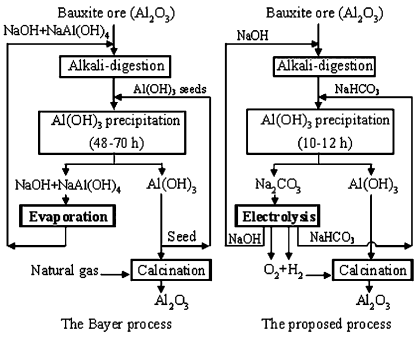

Efficiency doubles: The electrolysis of sodium carbonate generates concentrated caustic soda for bauxite ore digestion, sodium bicarbonate for aluminum hydroxide precipitation, and hydrogen and oxygen for the hydroxide calcination. Consequently, an efficient and sustainable production process of alumina from bauxite is proposed and the overall production efficiency is increased by 111% as compared with the Bayer process (see picture).

Sustainable Chemistry

Z. Yu, Y. Chen, Y. Niu, Y. Tang, P. Wan,* Z. Lv, X. J. Yang* ——— 11719 – 11723

Efficient and Sustainable Production of Alumina by Electrolysis of Sodium Carbonate

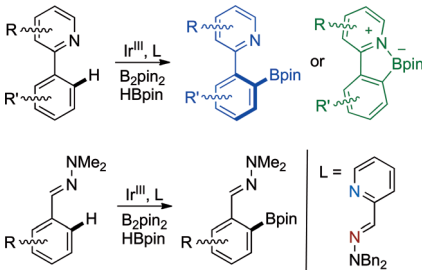

The hemilabile character of 2-pyridyl carbaldehyde hydrazones as N,N bidentate ligands is key to performing regioselective Ir^{III}-catalyzed *ortho* borylations of 2-aryl pyridines (isoquinolines) and aromatic *N*,*N*-dimethylhydrazones (see scheme; pin = pinacol, Bn = benzyl). Internal "ate" complexes or products free from N–B interactions are formed depending on the steric properties of the substrates.

Synthetic Methods

A. Ros, B. Estepa, R. López-Rodríguez, E. Álvarez, R. Fernández,* J. M. Lassaletta* ——— 11724 – 11728

Use of Hemilabile N,N Ligands in Nitrogen-Directed Iridium-Catalyzed Borylations of Arenes

Contents

Chirality

P. K. Hashim, N. Tamaoki* ——— 11729 – 11730

Induction of Point Chirality by *E*/*Z* Photoisomerization

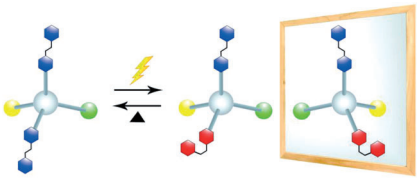

Shining a light on it: *E*/*Z* photoisomerization generates an asymmetric center and the corresponding separable enantiomers in an azobenzene-based prochiral molecule. This asymmetric center is formed by light-induced changes to the substituents on the central atom, and *Z*/*E* thermal isomerization regenerates the initial symmetry in the molecule. This switching of the asymmetry can be performed repeatedly.

Molecular Imprinting

G. Pan, Y. Zhang, Y. Ma, C. Li, H. Zhang* ——— 11731 – 11734

Efficient One-Pot Synthesis of Water-Compatible Molecularly Imprinted Polymer Microspheres by Facile RAFT Precipitation Polymerization

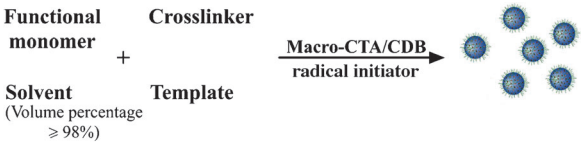

Narrowly dispersed water-compatible molecularly imprinted polymer (MIP) microspheres with surface-grafted hydrophilic polymer brushes were synthesized by RAFT precipitation polymerization (RAFTPP) mediated by hydrophilic macromolecular chain-transfer agents (Macro-CTA). The easy availability of hydrophilic Macro-CTAs and the versatility of the RAFTPP technique make it a general and promising strategy. CDB = cumyl dithiobenzoate.

Amido Complexes

I. Mena, M. A. Casado,* P. García-Orduña, V. Polo, F. J. Lahoz, A. Fazal, L. A. Oro* ——— 11735 – 11738

Direct Access to Parent Amido Complexes of Rhodium and Iridium through N–H Activation of Ammonia

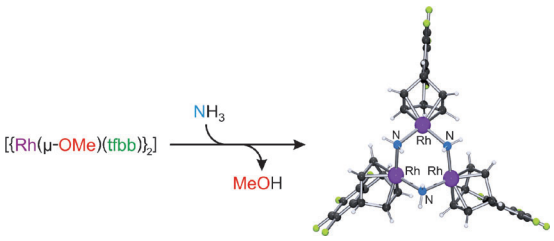

Simplicity! A direct entry to amido rhodium and iridium complexes was easily achieved by reaction of gaseous ammonia with alkoxo-bridged precursors under very mild conditions. This new approach allowed the high-yield access for the first time to elusive [Rh-NH_2] complexes.

Dye-Sensitized Solar Cells

X. Xin, M. He, W. Han, J. Jung, Z. Lin* ——— 11739 – 11742

Low-Cost Copper Zinc Tin Sulfide Counter Electrodes for High-Efficiency Dye-Sensitized Solar Cells

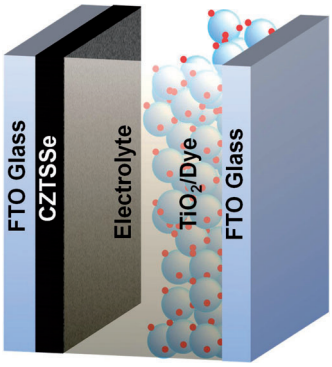

A copper zinc tin sulfide (CZTS) semiconductor can be used as an effective counter-electrode (CE) material in place of platinum metal, yielding low-cost, high-efficiency dye-sensitized solar cells (DSSCs). CZTS nanocrystals were synthesized and then spin-coated on fluorine-doped tin oxide (FTO) glass. After selenization, the power conversion efficiency of the resulting DSSC was comparable that with a Pt CE.

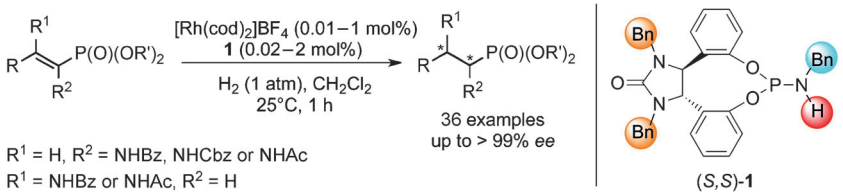

Synthetic Methods

J. Zhang, Y. Li, Z. Wang, K. Ding* ——— 11743 – 11747

Asymmetric Hydrogenation of α- and β-Enamido Phosphonates: Rhodium(I)/Monodentate Phosphoramidite Catalyst

High efficiency and enantioselectivity have been achieved in the Rh^{I}-catalyzed asymmetric hydrogenation of α- and β-enamido phosphonates using a monophosphoramidite as the chiral ligand (see scheme; cod = 1,5-cyclooctadiene), thus affording the optically active amino phosphonates with a turnover frequency of up to 1800 h^{-1} and high *ee* values.

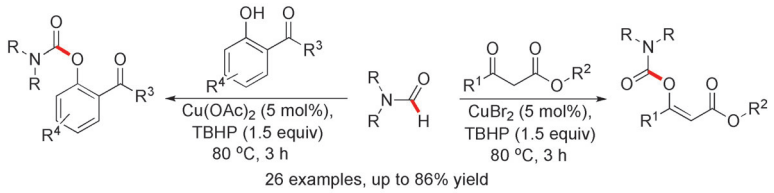

Oxidative Coupling

G. S. Kumar, C. U. Maheswari, R. A. Kumar, M. L. Kantam, K. R. Reddy* ——— 11748 – 11751

Copper-Catalyzed Oxidative C–O Coupling by Direct C–H Bond Activation of Formamides: Synthesis of Enol Carbamates and 2-Carbonyl-Substituted Phenol Carbamates

Formamide C–H bond activation has been achieved under oxidative conditions, using a copper catalyst and *tert*-butyl hydroperoxide (TBHP) as the external oxidant (see scheme). This oxidative coupling of a range of dialkyl formamides provides an easy, phosgene-free route for the selective synthesis of *Z*-enol carbamates and 2-carbonyl-substituted phenol carbamates in high yields.

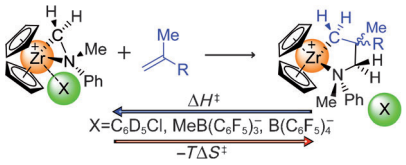

NMR Spectroscopy

L. Rocchigiani, G. Ciancaleoni, C. Zuccaccia,* A. Macchioni* ——— 11752 – 11755

Low-Temperature Kinetic NMR Studies on the Insertion of a Single Olefin Molecule into a Zr–C Bond: Assessing the Counterion–Solvent Interplay

Sticky counterions: Low-temperature kinetic NMR studies were performed to determine $\Delta H^{\ddagger}$ and $\Delta S^{\ddagger}$ values for the insertion of a single 2-methyl-1-heptene molecule into a Zr–C bond of $[Cp_2Zr(\eta^2\text{-}CH_2NMePh)][X]$ (**1a**: $X^- = MeB(C_6F_5)_3^-$, **1b**: $B(C_6F_5)_4^-$) in [D_8]toluene and a 1:1 mixture of [D_8]toluene and [D_5]chlorobenzene. Both activation parameters critically depend on the interplay of the counterion and the solvent.

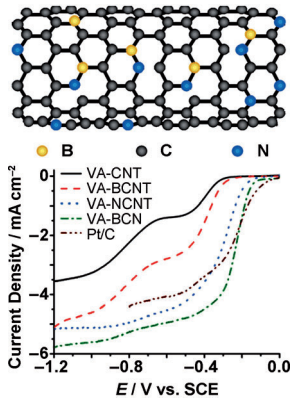

Oxygen Reduction

S. Wang, E. Iyyamperumal, A. Roy, Y. Xue, D. Yu, L. Dai* ——— 11756 – 11760

Vertically Aligned BCN Nanotubes as Efficient Metal-Free Electrocatalysts for the Oxygen Reduction Reaction: A Synergetic Effect by Co-Doping with Boron and Nitrogen

A single-compound source of B, C, and N was used for the growth of vertically aligned BCN (VA-BCN) nanotubes (NTs). Owing to a synergetic effect of co-doping of C nanotubes (CNTs) with N and B, the VA-BCN NTs show significantly improved electrocatalytic activity (e.g., current density) for the oxygen reduction reaction compared to undoped VA-CNTs, CNTs doped with only B or N (VA-BCNT, VA-NCNT), and a commercial Pt/C electrocatalyst (see picture).

Contents

Hindered Rotations

G. K. S. Prakash,* F. Wang, M. Rahm, J. Shen, C. Ni, R. Haiges, G. A. Olah* ——— **11761 – 11764**

On the Nature of C–H···F–C Interactions in Hindered CF_3–C(sp^3) Bond Rotations

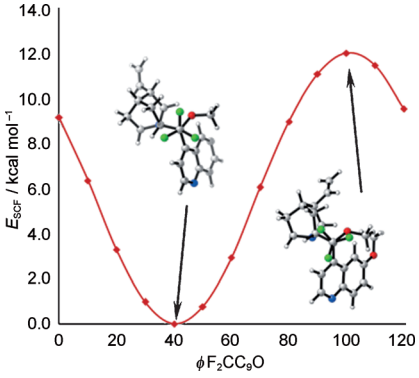

In cinchona alkaloid-based scaffolds, hindered CF_3 rotations have been observed. The variation in barrier heights for the CF_3 rotations is controlled by the corresponding entropic changes when the substituents are changed from an allyl to a bulky 9-methylanthracenyl group. Quantum chemical and experimental studies have shown that the noncovalent C3′–H1···F–C interactions in the studied cases possess a weak hydrogen bonding-like character.

Nanospheres

A.-H. Lu,* T. Sun, W.-C. Li, Q. Sun, F. Han, D.-H. Liu, Y. Guo ——— **11765 – 11768**

Synthesis of Discrete and Dispersible Hollow Carbon Nanospheres with High Uniformity by Using Confined Nanospace Pyrolysis

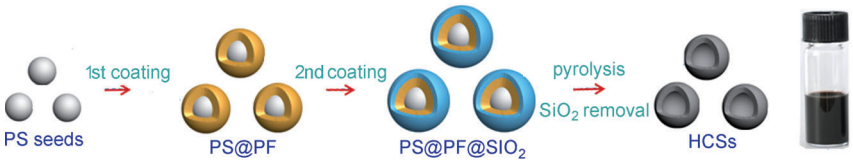

Many spheres of influence: Surface coating of monodisperse polystyrene (PS) nanosphere seeds with a phenol-containing polymer (PF) and then silica forms a dual core–shell structure PS@PF@SiO_2 (see picture). Subsequent pyrolysis results in discrete, dispersible, and uniform hollow carbon nanospheres (HCSs). The outer silica shell serves as a nanoreactor and thus prevents the polymer and carbon layers from conglutination and sintering.

Biomimetic Cell Capture

J. H. Myung, K. A. Gajjar, J. Saric, D. T. Eddington, S. Hong* ——— **11769 – 11772**

Dendrimer-Mediated Multivalent Binding for the Enhanced Capture of Tumor Cells

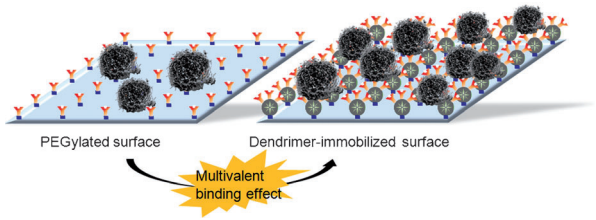

A naturally occurring multivalent binding effect is manipulated by engineering cell capture surfaces using dendrimers. The enhanced binding through the multivalent effect significantly improves detection of tumor cells. This improvement can be potentially translated into clinically significant detection of circulating tumor cells from the blood of cancer patients.

Organocatalysis

H. Xie, Y. Zhang, S. Zhang, X. Chen, W. Wang* ——— **11773 – 11776**

Bifunctional Cinchona Alkaloid Thiourea Catalyzed Highly Efficient, Enantioselective Aza-Henry Reaction of Cyclic Trifluoromethyl Ketimines: Synthesis of Anti-HIV Drug DPC 083

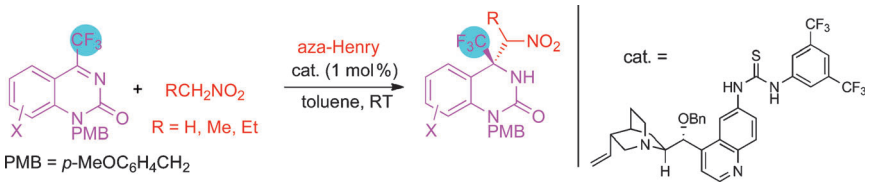

PMB = p-$MeOC_6H_4CH_2$

Highly efficient: The title reaction provides biologically interesting chiral trifluoromethyl dihydroquinazolinone frameworks in high yields (up to 97%) and with high enantioselectivities (up to 98% *ee*), using as low as 1 mol% of catalyst (see scheme). Moreover, anti-HIV drug candidate DPC 083 was efficiently synthesized using the highly enantioselective aza-Henry reaction as a key step.

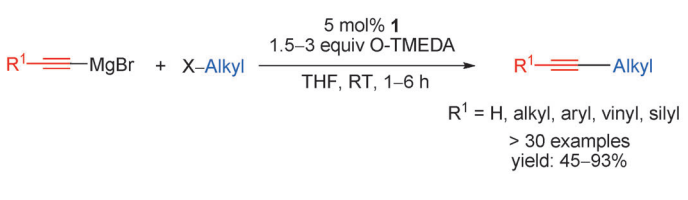

In a pinch: The nickel pincer complex **1** catalyzes the cross-coupling of the title compounds with remarkable substrate scope and functional group tolerance. A nickel/alkynyl species was isolated and shown to be catalytically competent. THF = tetrahydrofuran, O-TMEDA = bis[2-(*N*,*N*-dimethylaminoethyl)] ether.

Synthetic Methods

O. Vechorkin, A. Godinat, R. Scopelliti, X. L. Hu* ——— **11777 – 11781**

Cross-Coupling of Nonactivated Alkyl Halides with Alkynyl Grignard Reagents: A Nickel Pincer Complex as the Catalyst

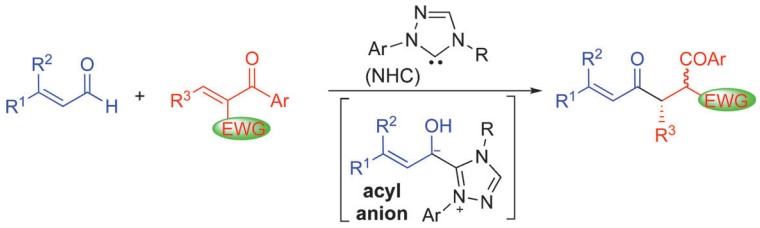

New trick for an old cat.: Triazolium-based N-heterocyclic carbenes (NHCs) catalyze the selective generation of acyl anion equivalents for the title reaction. The stereoelectronic properties of the enal-derived Breslow intermediates and the unique reactivity of the modified chalcones are crucial for the Stetter reactions to occur. EWG = electron-withdrawing group.

Organocatalysis

X. Fang, X. Chen, H. Lv, Y. R. Chi* ——— **11782 – 11785**

Enantioselective Stetter Reactions of Enals and Modified Chalcones Catalyzed by N-Heterocyclic Carbenes

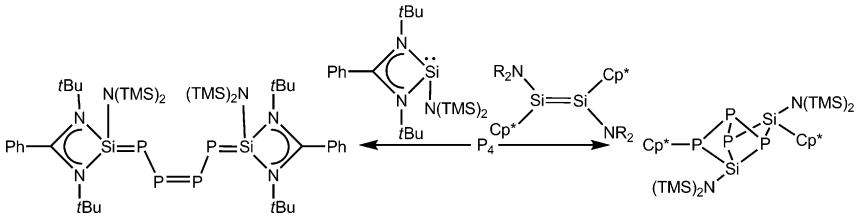

An acyclic P_4 chain supported by a silicon-substituted amidinato ligand was formed from the reaction of $PhC(NtBu)_2SiN(TMS)_2$ with P_4 (TMS = Me_3Si). This is the first example of an acyclic Si—P chain that contains 6π electrons. When the benzamidinato moiety was replaced with Cp* (Cp* = Me_5C_5), an unusual silicon–phosphorus cage surprisingly formed (see scheme).

P_4 Activation

S. Khan, R. Michel, S. S. Sen, H. W. Roesky,* D. Stalke* **11786 – 11789**

A P_4 Chain and Cage from Silylene-Activated White Phosphorus

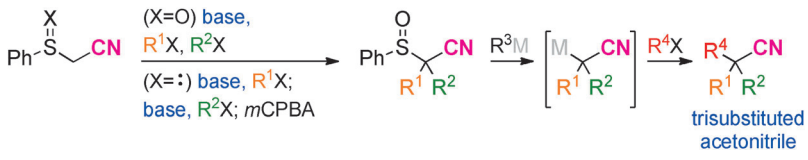

Triple alkylation: Phenylsulfinyl- and phenylthioacetonitrile can function as trianion equivalents of acetonitrile by sequential alkylation and sulfinyl–metal exchange (see scheme; *m*CPBA = *meta*-chloroperoxybenzoic acid). The metalated nitriles alkylate a range of electrophiles to obtain nitriles with quaternary centers. The sulfinyl–metal exchange proceeds under very mild conditions and has a high functional-group tolerance.

Quaternary Carbon Centers

D. Nath, F. F. Fleming* — **11790 – 11793**

Nitrile Alkylations through Sulfinyl–Metal Exchange

Contents

18-Electron Rule

M. S. G. Ahlquist,*
P.-O. Norrby* ——— **11794 – 11797**

Dispersion and Back-Donation Gives Tetracoordinate $[Pd(PPh_3)_4]$

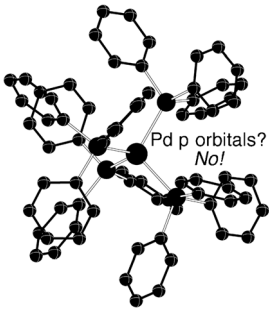

18e R.I.P. The apparent compliance of $[Pd(PPh_3)_4]$ ("tetrakis") with the 18-electron rule is not due to an electronic preference on the central metal. Pd is valence-saturated already by two ligands. Further ligand addition gives a minor energy gain, and is only possible due to strong back-bonding. Dispersion corrections are needed for properly describing the interactions between the ligands.

Heterocycles

L. L. W. Cheung, Z. He, S. M. Decker, A. K. Yudin* ——— **11798 – 11802**

Skeletal Fusion of Small Heterocycles with Amphoteric Molecules

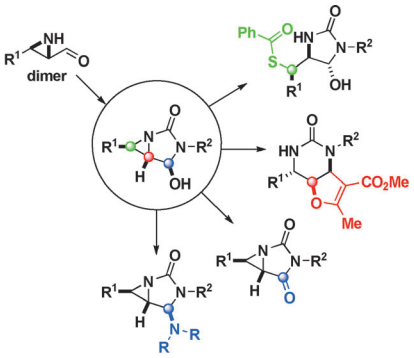

Latched on: A new class of hydantoin derivatives with three contiguous stereocenters was prepared from a [3+2] annulation involving amphoteric aziridine aldehydes and isocyanates and further converted to a series of densely functionalized hetercycles, which are difficult to synthesize using established methods. The results highlight the potential of (1,3) amphoteric molecules to construct heterocyclic scaffolds using trivial starting materials.

Supporting information is available on www.angewandte.org (see article for access details).

A video clip is available as Supporting Information on www.angewandte.org (see article for access details).

This article is available online free of charge (Open Access)

Service

Spotlight on Angewandte's Sister Journals ——— ***11562 – 11564***

Preview ——— ***11803***